Clays and Clay Minerals, Vol. 69, No. 4:453–462, 2021

RELEASE OF Mg AND Fe FROM THE OCTAHEDRAL SHEETS DURING THE TRANSFORMATION OF MONTMORILLONITE INTO KAOLINITE

Shangying Li[1,2], Qi Tao[1,3], Lingya Ma[1,3]*, Chaoqun Zhang[1,2], Yixuan Yang[1,2], Peixin Du[5], Jiacheng Liu[5], and Jianxi Zhu[1,2,3]

[1]Key Laboratory of Mineralogy and Metallogeny, Chinese Academy of Sciences & Guangdong Provincial Key Laboratory of Mineral Physics and Materials, Guangzhou Institute of Geochemistry, Guangzhou 510640, China
[2]University of Chinese Academy of Sciences, Beijing 100049, China
[3]CAS Center for Excellence in Deep Earth Science, Guangzhou 510640, China
[4]State Key Laboratory of Lunar and Planetary Sciences, Macau University of Science and Technology, Macau, China
[5]Division of Earth and Planetary Science & Laboratory for Space Research, The University of Hong Kong, Hong Kong, China

Abstract—Isomorphous substitutions of Mg and Fe for Al generally appear in the octahedral sheets of montmorillonite, whereas they are infrequent in kaolinite. Therefore, the release of Mg and Fe from the octahedral sheets probably happens during the transformation of montmorillonite into kaolinite, which could affect the migration of Mg and Fe from clay minerals into surrounding environments. The objective of the current study was to investigate the relationship between Mg and Fe release during the transformation of montmorillonite into kaolinite. The results showed that the d_{060} value of clay minerals decreased slightly, and the intensities of both the AlMg–OH and AlFe–OH bending vibrations also decreased gradually. In addition, the (Mg+Fe)/Al (major octahedral ions) atomic ratio of kaolinite was lower than that of montmorillonite, especially in identical hydrothermal products. These results indicated that Mg and Fe ions were released progressively from the octahedral sheets during the transformation of montmorillonite into kaolinite. Moreover, the changed relative concentrations of Mg and Fe ions in the supernatant solutions after hydrothermal reactions suggested a random distribution of Mg and/or Fe in the octahedral sheets of the montmorillonite. These results improve understanding of the release relationship between Mg and Fe during clay mineral evolution and of the distribution of these two ions in the octahedral sheets, as well as the chemical composition of clay minerals as an indicator of geological environments.

Keywords—Fe · Kaolinite · Mg · Montmorillonite · Octahedral sheet · Release

INTRODUCTION

The migration of elements during the evolution of clay minerals plays a critical role in controlling the chemical compositions of surface water and soils and in forming secondary minerals because clay minerals are ubiquitous in various environments on the Earth. Studies have focused more on the transformation mechanisms of clay minerals over the past decades but less on the migration of elements in these transformation processes (Dudek et al., 2006; Hong et al., 2012, 2015; Ryan & Huertas, 2013; Li et al., 2020). One of the most common evolutions of clay minerals, kaolinization of smectites (e.g. montmorillonite and beidellite), generally occurs in weathering environments on the Earth's surface, with the interstratified kaolinite-smectite (K-S) minerals acting as intermediate phases during these processes (Dudek et al., 2006; Hong et al., 2012; Oliveira et al., 2018; Li et al., 2020).

In smectites, the isomorphous substitutions of Mg^{2+}, Fe^{2+}, and Fe^{3+} for Al^{3+} in the octahedral sheets and/or the substitutions of Al^{3+} and Fe^{3+} for Si^{4+} in the tetrahedral sheets are common, and produce a net negative layer charge (Sainz-Diaz et al., 2000; He et al., 2014; Baron et al., 2016; Ilgen et al., 2017). However, the octahedral and tetrahedral cations of kaolinite are almost all Al^{3+} and Si^{4+}, respectively, indicating that isomorphous substitution rarely happens in kaolinite (Aparicio & Galan, 1999; He et al., 2003). The kaolinization of smectites could result, therefore, in the release of Mg and Fe from the octahedral sheets of smectites into the surrounding environments (Hong et al., 2015).

The kaolinization of smectites occurs generally in acidic environments (Dudek et al., 2006, 2007; Ryan & Huertas, 2013; Hong et al., 2015). These settings benefit the dissolution of smectites and the release of Mg and Fe (Dudek et al., 2006; Rozalén et al., 2008). A previous study indicated that kaolinite domains contained less Mg than smectite domains and illite domains, which suggested that Mg was released from precursor minerals when smectites and illite transformed into kaolinite (Hong et al., 2015). In addition, the release of elements from precursor minerals could give rise to the precipitation of secondary minerals such as brucite and goethite (Rozalén et al., 2009; Ryan & Huertas, 2013). Nevertheless, a tiny proportion of Mg and Fe in kaolinite could be inherited from the precursor octahedral sheets after the structural transformation (Ryan & Huertas, 2013). Doubt remains as to the relationship between Mg and Fe released from the octahedral sheets into the surrounding environments throughout the kaolinization of montmorillonite under acidic conditions.

The objective of the present study, therefore, was to investigate the release relationship between Mg and Fe in the process of

* E-mail address of corresponding author: malingya@gig.ac.cn
DOI: 10.1007/s42860-021-00138-5

kaolinization of montmorillonite under hydrothermal conditions. The starting material and solid phases obtained were characterized comprehensively with X-ray diffraction (XRD), Fourier-transform infrared spectroscopy (FTIR), Mössbauer spectroscopy, ^{27}Al magic angle spinning nuclear magnetic resonance spectroscopy (^{27}Al MAS NMR), high-resolution transmission electron microscopy (HRTEM), and energy-dispersive X-ray spectroscopy (EDS). The concentrations of Mg and Fe in the supernatant solutions corresponding to the hydrothermal products were measured with inductively coupled plasma atomic emission spectroscopy (ICP-AES). The hypothesis was that the Mg and Fe ions are distributed randomly within the octahedral sheets of the montmorillonite and exhibit a similar tendency to be released progressively during the transformation to kaolinite.

MATERIALS AND METHODS

Starting Material and Hydrothermal Experiments

Montmorillonite (Mnt) as the precursor mineral to be transformed into kaolinite (Li et al., 2020) was obtained from a mineral deposit near Chifeng, Inner Mongolia Autonomous Region, China, which consisted mainly of Mnt. The chemical composition was determined using X-ray fluorescence spectroscopy (XRF), and the results were shown in a previous study (Li et al., 2020). The cation-exchange capacity (CEC) of Mnt was 110.73 mmol/100 g, determined with UV-Vis spectrophotometry of using $[Co(NH_3)_6]^{3+}$ (Alfa Aesar, A15470) as the exchanging cation (Hu et al., 2000; He et al., 2014). The Mnt was not treated chemically before the hydrothermal experiments. The detailed procedures of hydrothermal experiments were described previously (Li et al., 2020). In brief, the sample containing Mnt was placed in a solution containing $AlCl_3$ (Guangzhou Chemical Reagent Factory, China). The resulting pH value of suspension was adjusted to 3 and then treated hydrothermally at 250°C under autogenous water pressure for various times (from 1 to 8 days). The suspension obtained was centrifuged at 4000 rpm (3000×*g*) for 10 min, and the supernatant solution was collected to determine the concentrations of Mg and Fe. The solid product was washed several times to remove redundant ions and dried at 80°C for 24 h and finally marked as Mnt-X, where X stands for hydrothermal duration time (e.g. 1d = 1 day).

Methods

XRD. XRD analyses were performed on a Bruker D8 Advance diffractometer (Karlsruhe, Germany) with Ni-filtered CuKα radiation (λ = 0.154 nm, 40 kV, and 40 mA) at Guangzhou Institute of Geochemistry (GIG), Chinese Academy of Sciences (CAS) (Guangzhou, China). All of the XRD patterns of Mnt and its hydrothermal products were collected between 3 and 70°2θ at a scanning rate of 3°2θ/min.

FTIR. FTIR spectra were recorded on a Bruker Vertex-70 Fourier-transform infrared spectrometer (Ettlingen, Germany) using the KBr pressed-disk technique at GIG, CAS (Guangzhou, China). Each KBr pellet was prepared by mixing 0.9 mg of the sample with 80 mg of spectroscopic-grade KBr powder which was then well ground in an agate mortar for 15 min. Then the specimen was pressed for 5 min at 10 kbar. Finally, the mixture was heated under a lamp for 3 min to reduce adsorbed water before the FTIR measurement. All of the spectra were collected in the 4000–400 cm^{-1} range with 64 scans and a resolution of 4 cm^{-1} (He et al., 2017).

Mössbauer spectroscopy. The Mössbauer spectrum of Mnt was recorded on a WSS-10 spectrometer (Silver Double Limited, USA) at 298 K at GIG, CAS (Guangzhou, China). The velocity drive transducer operated in a triangular waveform mode over energy ranges of ±15 mm/s, with a 25 mCi ^{57}Co source dispersed as 10 wt.% in a thin Rh foil. Spectral deconvolution of the Mössbauer spectrum obtained was fitted using the doublet having a Lorentzian line shape (Decarreau & Bonnin, 1986; Baron et al., 2017).

^{27}Al MAS NMR. ^{27}Al MAS NMR spectra were recorded on a Bruker AVANCE III 600 spectrometer (Rheinstetten, Germany) at the resonance frequencies of 156.4 MHz at a high magnetic field laboratory, CAS (Hefei, China). A 4 mm HX double-resonance MAS probe was used to measure ^{27}Al MAS NMR at a sample spinning rate of 14 kHz. The spectra were recorded by a small-flip angle technique with a pulse length of 0.5 μs (<π/12) and a 1 s recycle delay. The chemical shift of the ^{27}Al MAS NMR spectrum was referenced to 1 M aqueous $Al(NO_3)_3$ (Zhang et al., 2017).

HRTEM. The oriented samples Mnt, Mnt-4d, and Mnt-8d were embedded in epoxy resin (Dong et al., 1998) and then dried at 100°C for 3 h to observe the lattice fringes of montmorillonite and kaolinite along the [001] direction. Subsequently, ultrathin sections with a thickness of ~75 nm were obtained with a diamond knife operating on a Lecia EM UC7 ultramicrotome (Wetzlar, Germany) at GIG, CAS. The specimen was placed on a carbon-coated copper micro-grid for TEM observation (Ji et al., 2018; Li et al., 2020). TEM was performed on an FEI Talos F200S microscope (Brno, Czech Republic) equipped with an X-ray energy-dispersive detector at GIG, CAS (Guangzhou, China). The instrument was operated at an accelerating voltage of 200 kV.

ICP-AES. Mg and Fe in the starting material were dissolved into solution during the hydrothermal treatment process (Dudek et al., 2007). The concentrations of Mg and Fe in the supernatant solutions of hydrothermal products were determined using a Thermo Scientific iCAP 7000 inductively coupled plasma atomic emission spectrometer (Bremen, Germany) at Ji'nan University (Guangzhou, China). Each supernatant solution was diluted 10 times to reduce the concentrations of the ions before ICP-AES analysis.

https://doi.org/10.1007/s42860-021-00138-5 Published online by Cambridge University Press

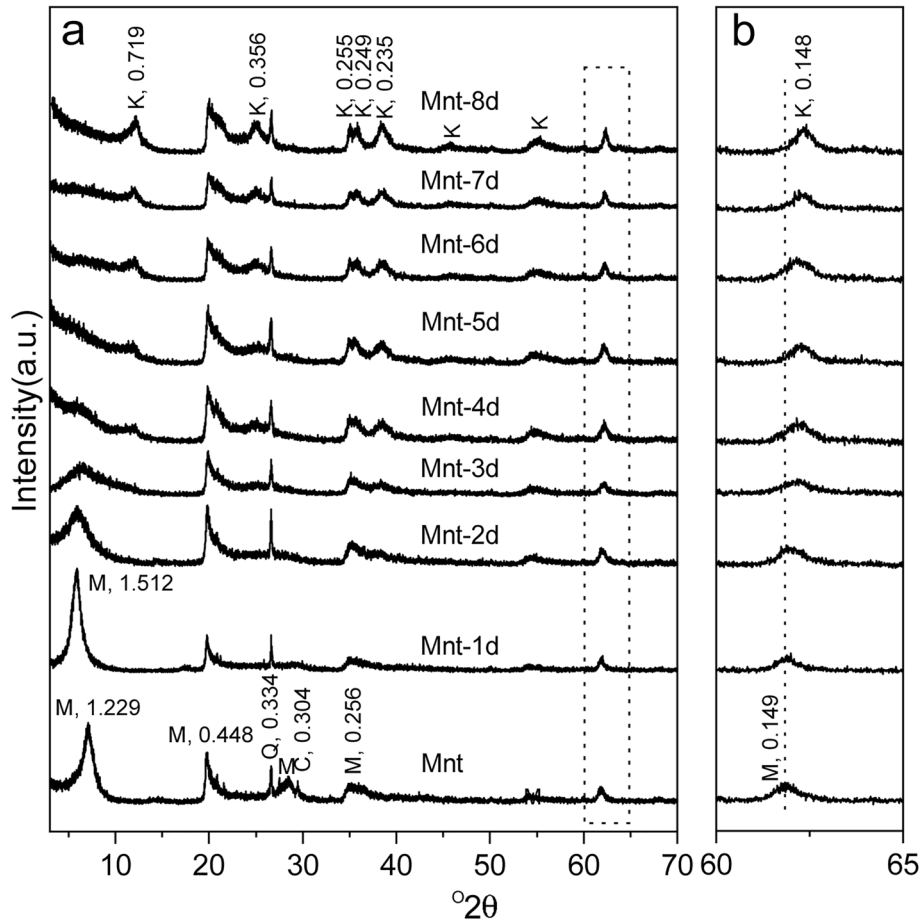

Fig. 1. XRD patterns of sample Mnt and its hydrothermal products after various duration times. The hydrothermal products were obtained from 1 day (Mnt-1d) to 8 days (Mnt-8d). Image **b** is a magnification of the region surrounded by the dotted rectangle in image **a**

RESULTS AND DISCUSSION

Characteristics of Starting Materials and their Hydrothermal Products

XRD patterns. The powder XRD patterns of Mnt and hydrothermal products are shown in Fig. 1a. Before the hydrothermal treatment, the d_{001} value of montmorillonite was 1.229 nm, suggesting that Na^+ was the dominant cation in the interlayers on the basis of XRF results (Li et al., 2020). Thus, the precursor mineral that was used in the present study was Na-montmorillonite. The basal spacing value of montmorillonite increased to 1.512 nm after a 1-day treatment (Mnt-1d), implying that Al^{3+} in the acidic solution entered into the interlayer space (Li et al., 2020). For the hydrothermal products from Mnt-4d to Mnt-8d, one newly appeared reflection with a *d* value of 0.719 nm was the characteristic 001 reflection of kaolinite (Dudek et al., 2006). With an extended duration of hydrothermal treatment, the intensities of the reflections related to montmorillonite decreased dramatically and almost disappeared after the 8-day hydrothermal treatment (Mnt-8d), whereas those of kaolinite increased. This indicated that the transformation from montmorillonite into kaolinite was virtually complete during the hydrothermal processes. It is noteworthy that the d_{060} value of clay minerals slightly decreased from 0.149 (in Mnt) to 0.148 nm (in Mnt-8d) with the increase in hydrothermal reaction time (Fig. 1b), indicating that some ions larger than Al were removed gradually from the octahedral sheets (Cuadros et al., 2009).

In all XRD patterns, the reflection with a *d* value of 0.334 nm was indicative of the existence of quartz (Schelz, 1976), the intensity of which showed no noticeable change, reflecting that quartz was relatively stable throughout the hydrothermal treatment. Hence, it can be used as an internal standard for calibrating the reflection positions of the clay minerals, especially the 060 reflections (Fig. 1b).

FTIR spectra. Kaolinite possesses inner-surface hydroxyls that montmorillonite does not. Such a difference could be distinguished by their FTIR spectra (Fig. 2). The structural –OH stretching vibrations of montmorillonite and/or kaolinite in the starting material and the hydrothermal products were recorded in the 3700 to 3600 cm^{-1} range. For Mnt, the Al_2–OH stretching vibration was relatively broad and located at ~3624

https://doi.org/10.1007/s42860-021-00138-5 Published online by Cambridge University Press

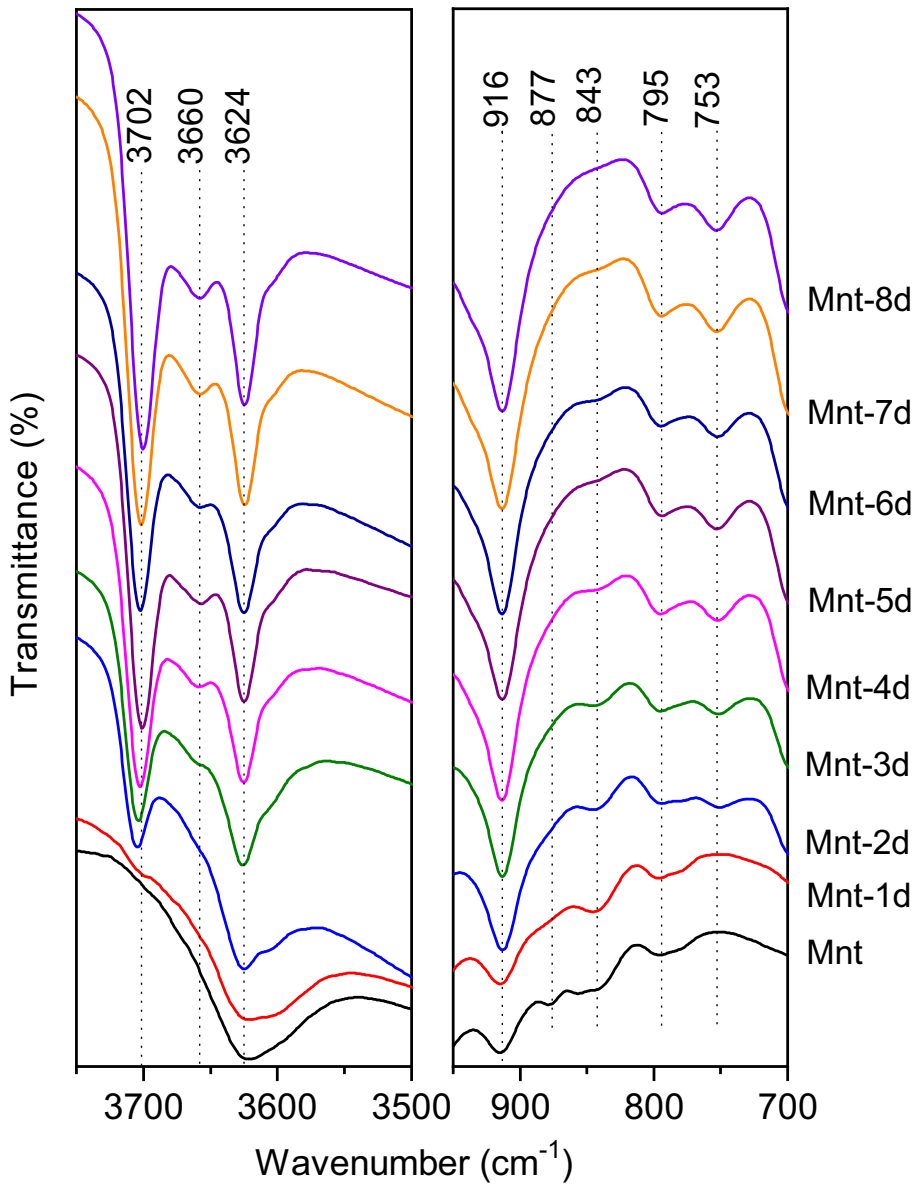

Fig. 2. FTIR spectra of starting material (Mnt) and its hydrothermal products after various duration times. The hydrothermal products were obtained from 1 day (Mnt-1d) to 8 days (Mnt-8d)

cm^{-1} (Dudek et al., 2007). A similar band also appeared in the FTIR spectra of hydrothermal products with a sharp shape, which resulted from the overlap with the inner Al_2–OH stretching vibration of the kaolinite subgroup minerals (Adazabra et al., 2017). Two new absorption bands at 3702 and 3660 cm^{-1} were ascribed to the inner surface Al_2–OH stretching vibrations of kaolinite in the hydrothermal products (except Mnt-1d), and their intensities gradually became stronger with the increase in hydrothermal duration time. Note that the band at 3702 cm^{-1} attributed to the Al_2–OH stretching vibration of kaolinite was displayed in the FTIR spectrum of Mnt-2d, indicating strongly the formation of kaolinite layers not detected by the XRD measurement (Ryan & Huertas, 2013). The appearance of such an absorption band suggested that FTIR analysis is much more sensitive to the formation of kaolinite layers than the XRD method, because the FTIR is used to detect directly the chemical bonds of minerals, and is much less dependent on the periodicity of a crystal lattice than the XRD method is. Other, not easily observed, features included other structural –OH (e.g. AlMg–OH and AlFe–OH) stretching vibrations in the clay minerals, owing to their low proportions in the

https://doi.org/10.1007/s42860-021-00138-5 Published online by Cambridge University Press

octahedral sheets, as well as the overlapping bands of complicated Al_2–OH stretching vibrations and/or –OH stretching vibrations in the adsorbed water.

FTIR spectra are also powerful for distinguishing kaolinite from halloysite (7 Å). In this study, the FTIR spectra indicated that poorly crystallized kaolinite rather than halloysite (7 Å) formed in the hydrothermal products, because the Al_2–OH stretching bands of halloysite (7 Å) always located at ~3700 and 3630 cm^{-1}, and the other visible absorption bands were absent between them (Pansu & Gautheyrou, 2006; Zhang et al., 2012; He et al., 2017). Moreover, two bands at 795 and 753 cm^{-1} were of nearly equal intensity (Fig. 2), also suggesting that the neo-formed product was kaolinite rather than halloysite (7 Å) because the former band is weaker than the latter 1 in halloysite (Pansu & Gautheyrou, 2006).

In the low-frequency regions, the Al_2–OH bending vibration of montmorillonite and/or kaolinite was located at 916 cm^{-1} and its intensity also increased with the extension of hydrothermal duration time due to the progressive transformation of montmorillonite into kaolinite. Notice also that weak AlMg–OH and AlFe–OH bending vibrations in precursor montmorillonite appeared at 877 and 843 cm^{-1}, respectively (Fig. 2) (Cuadros & Dudek, 2006; Dudek et al., 2007). They gradually weakened even further with the extension of hydrothermal treatment time and nearly disappeared in sample Mnt-8d (Fig. 2).

Mössbauer spectrum. Theoretically, Fe^{3+} could occupy the sites in the octahedral sheets and the tetrahedral sheets of montmorillonite, and Fe^{2+} could occupy the sites in the octahedral sheets. Although the Fe content was small, as indicated by the XRF results (Li et al., 2020), the valence and occupancy of Fe in either tetrahedral or octahedral sheets of precursor montmorillonite were able to be determined according to the isomer shift and quadrupole splitting values of the deconvolution of the Mössbauer spectrum (Baron et al., 2017). In the current study, the Mössbauer spectrum showed one doublet, with isomer shift and quadrupole splitting of 0.33 and 0.61 mm/s, respectively (Fig. 3), indicating that most of the iron occurred as Fe^{3+} in the octahedral sheets (Decarreau & Bonnin, 1986; Baron et al., 2017). This observation was consistent with the FTIR result of precursor montmorillonite (Fig. 2) and suggested that Fe^{3+} occupied preferentially the octahedral sheet of montmorillonite.

^{27}Al MAS NMR spectrum. The ^{27}Al MAS NMR spectrum of montmorillonite displayed a strong signal of 6-coordinated Al (^{VI}Al) at ~5.01 ppm and a weak one from 4-coordinated Al (^{IV}Al) at ~61.62 ppm (Fig. 4). After one-day of treatment (Mnt-1d), the weak ^{IV}Al signal disappeared, which probably resulted from the dissolution of montmorillonite particles containing a small amount of isomorphous substitution of Al^{3+} for Si^{4+} in the tetrahedral sheets. Extension of the hydrothermal treatment to eight-days created a sharp signal at ~6.34 ppm (Fig. 4), which was assigned to ^{VI}Al in the octahedral sheets of kaolinite (He et al., 2017).

The combined results of XRF (Li et al., 2020), Mössbauer, and ^{27}Al MAS NMR spectra inferred that the chemical formula of montmorillonite was $M^{+}_{0.54}(Si_{3.96}Al_{0.04})(Al_{1.25}Mg_{0.5}Fe_{0.25})O_{10}(OH)_2{\cdot}nH_2O$, where both Mg and Fe

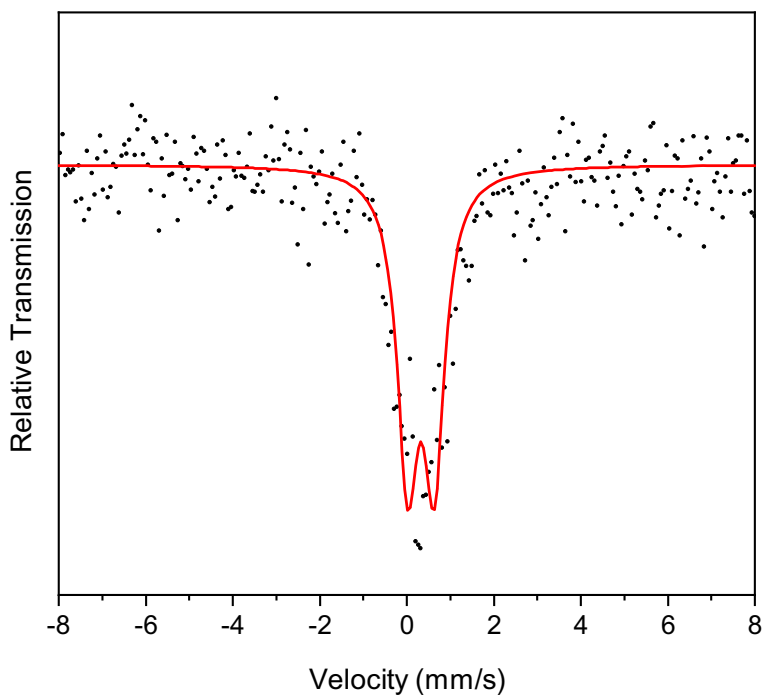

Fig. 3. Mössbauer spectrum at 298 K of starting material (Mnt). The spectral deconvolution was optimal using one doublet

https://doi.org/10.1007/s42860-021-00138-5 Published online by Cambridge University Press

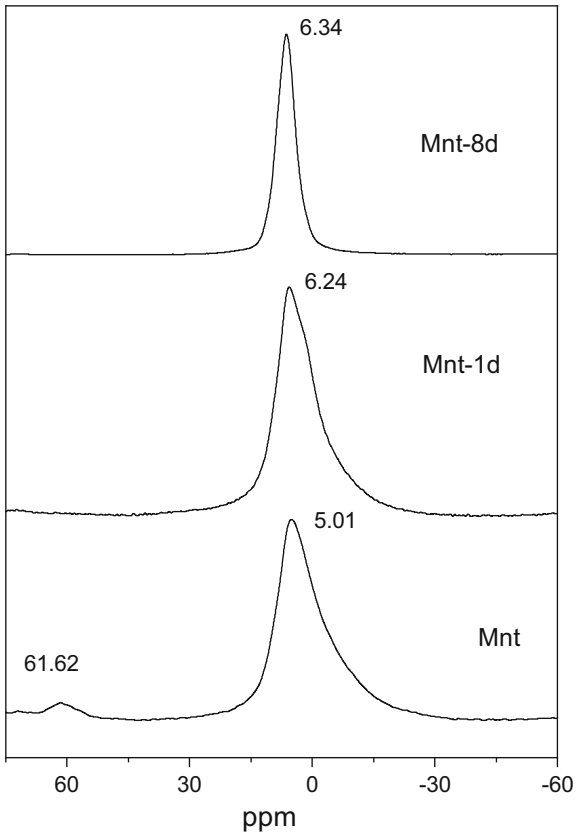

Fig. 4. ^{27}Al MAS NMR spectra of starting material (Mnt) and hydrothermal products after 1 day (Mnt-1d) and 8 days (Mnt-8d)

occupied the octahedral sheets, and the atomic ratio of (Mg+Fe)/Al (major octahedral ions) was ~0.58.

HRTEM observations and EDS analyses. Precursor montmorillonite and product kaolinite were easily identified under HRTEM observations because these two clay minerals exhibited different lattice-fringe thicknesses along their own [001] directions (Fig. 5). The HRTEM image of Mnt showed that montmorillonite particles exhibited lattice fringes with a periodicity of ~1.0 nm due to the escape of interlayer water by electron beam heating (Fig. 5a and e) (Li et al., 2020). The EDS analysis of such montmorillonite domains indicated that these particles had significantly greater Si and Al contents as well as minor Mg and Fe (Fig. 6), and the (Mg+Fe)/Al atomic ratio was close to that (0.58) of Mnt by XRF determination. The XRD pattern showed that montmorillonite and kaolinite occurred simultaneously in sample Mnt-4d (Fig. 1a). Correspondingly, these two clay mineral phases were discovered during the HRTEM observations of this sample (Fig. 5b, c, f, and g). Among them, the lattice fringes representing montmorillonite had a periodicity of ~1.3 nm (Fig. 5f), suggesting the formation of hydroxy-Al polymers in the interlayers of montmorillonite (Ryan & Huertas, 2009; Li et al., 2020), which was consistent with the XRD test (Fig. 1a). Besides, kaolinite domains showed straight lattice fringes with ~0.7 nm thickness (Fig. 5c and g). The EDS analysis of sample Mnt-4d showed that the (Mg+Fe)/Al atomic ratio (0.20) of montmorillonite domains was greater than that (0.08) of kaolinite domains (Fig. 6b and c). In sample Mnt-8d, abundant lattice fringes with a periodicity of ~0.7 nm were observed (Fig. 5d and h), reflecting the large amount of kaolinite formed. The EDS analysis showed that these kaolinite domains contained trace amounts of Mg and Fe, and the (Mg+Fe)/Al atomic ratio (0.05) was also very low (Fig. 6d), which probably resulted from the adsorption of a very small amount of Mg and Fe ions onto the kaolinite particles rather than the preservation of these two ions in the octahedral sheets of newly formed kaolinite, because the pH of the hydrothermal experiments in the present study was very unfavorable to the formation of Mg- and Fe-hydroxide structures (Rozalén et al., 2008; Li et al., 2020).

ICP-AES analysis. The concentrations of Mg and Fe for Mnt-1d did not reflect exactly their release from precursor montmorillonite, because a small amount of Mg and Fe might be stored in a few other weakly crystallized or amorphous phases. However, the accumulated concentrations of both ions in the supernatant solution corresponding to each sample reflected their migrations from solid phases into solution, because all of the samples went through a similar initial hydrothermal treatment. Therefore, the release of Mg and Fe was also mirrored by their concentrations in the supernatant solutions after various hydrothermal reactions times (Fig. 7).

The concentrations of Fe and Mg were close and exhibited similar evolutionary tendencies during the montmorillonite kaolinization process. The relative concentrations of Mg and Fe changed, however. In stage 1 (1–4 days), the concentration of Mg was greater than that of Fe, whereas this relationship was reversed in stage 3 (6–8 days). Increased concentrations of Mg and Fe also indicated the gradual release of these two ions from octahedral sheets with changed release rates during montmorillonite kaolinization. The results showed that Mg and Fe started with a fast release from the solid phase (stage 1 in Fig. 7) and followed with a very slow rate indicated by their nearly constant concentrations (stage 2 in Fig. 7). The release ended at another fast rate as reflected by an increase in the concentrations of Mg and Fe during the timescale of the experiments (stage 3 in Fig. 7). Such changed concentrations and release rates of Mg and Fe resulted mainly from the different dissolution rates of montmorillonite with varied particle sizes and edge structures (Bray et al., 2015; Li et al., 2020). In stage 1, the release of Mg and Fe was probably derived from small montmorillonite particles always with a large proportion of rough edges, which exhibited a fast dissolution rate. Later, large montmorillonite particles would dissolve,

https://doi.org/10.1007/s42860-021-00138-5 Published online by Cambridge University Press

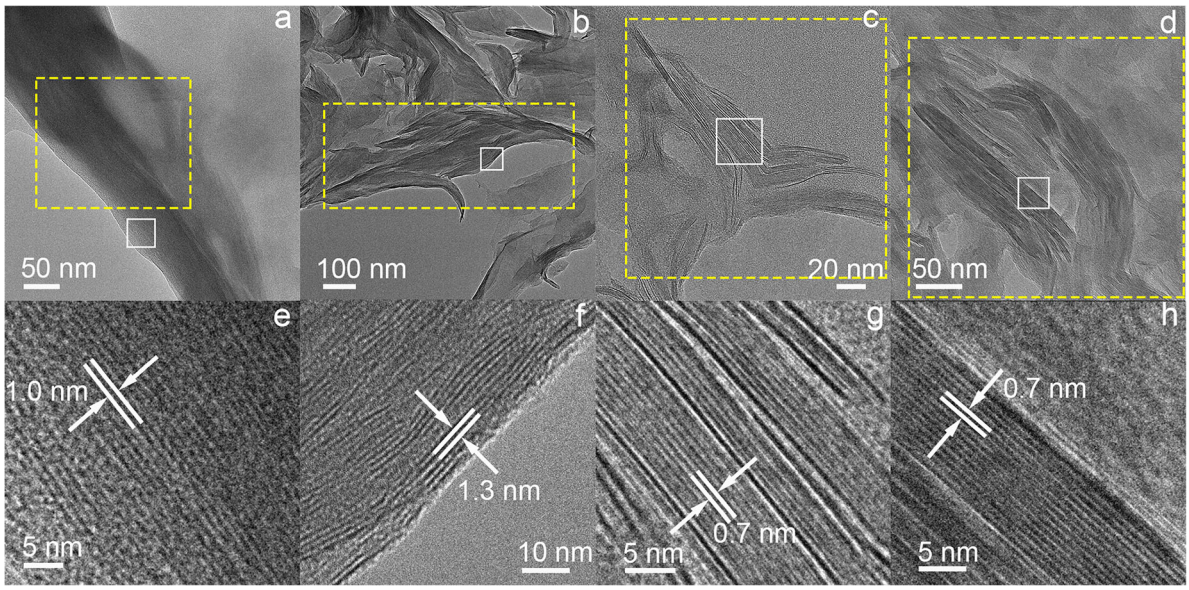

Fig. 5. TEM images of montmorillonite and kaolinite in the starting material (Mnt) and its hydrothermal products: **a** montmorillonite particle in sample Mnt; **b** montmorillonite particles in the hydrothermal product obtained from acidic solutions containing Al after 4 days (Mnt-4d); **c** kaolinite particle in sample Mnt-4d; **d** kaolinite particles in sample Mnt-8d. Images **e**, **f**, **g**, and **h** are the HRTEM images of the areas surrounded by the solid white squares in images **a**, **b**, **c**, and **d**, respectively

corresponding to the release of Mg and Fe in stages 2 and 3 (Fig. 7).

Release of Mg and Fe from the Octahedral Sheets of Precursor Montmorillonite

Based on the FTIR result, the absorption bands at 877 and 843 cm^{-1} corresponding to AlMg–OH and AlFe–OH bending vibrations, respectively, gradually became weak and eventually almost disappeared with the increase in hydrothermal reaction time (Fig. 2), reflecting the progressive release of octahedral Mg and Fe. Moreover, the XRD result showed that the d_{060} value of the clay minerals decreased slightly from 0.149 (in Mnt) to 0.148 nm (in Mnt-8d) with the increasing hydrothermal treatment time (Fig. 1b). This slight decrease in d_{060} was due to the release of Mg and Fe from the octahedral sheets because the *b* cell dimension of phyllosilicates is sensitive to the subtle changes in the radius of octahedral cations (cation radii: $Fe^{2+} > Mg^{2+} > Fe^{3+} > Al^{3+}$) (Cuadros et al., 2009; Cuevas et al., 2009; Doublier et al., 2010). Combined data from the HRTEM images and EDS analyses of sample Mnt-4d indicated that the (Mg+Fe)/Al atomic ratio of neo-formed kaolinite domains was smaller than that of montmorillonite domains (Figs 5 and 6). It also suggested that Mg and Fe were released when montmorillonite transformed into kaolinite. The ICP-AES result showed that the concentrations of Mg and Fe in the supernatant solutions increased with increasing hydrothermal treatment time (Fig. 7), consistent with XRD and FTIR results (Figs 1 and 2).

Results from the present study indicated that Mg and Fe in octahedral sheets were prone to be released from the clay minerals into the surrounding environments under the reaction condition of low pH, consistent with the studies on the natural samples (Dudek et al., 2006; Hong et al., 2015). Hence, kaolinite with small Mg and Fe contents could be the indicator reflecting the acidic conditions in which kaolinite forms. In the current study, the secondary Mg- and Fe-bearing minerals were not detected because the low pH and Mg and Fe concentrations prevented the precipitation of Mg- and Fe-bearing phases from solution. In addition, water is well known to be absent from the interlayers of kaolinite compared with montmorillonite. Therefore, the kaolinization of montmorillonite could drive some elements (e.g. Mg, Fe, and Si) into geological fluids and promote the release of interlayer water.

Distributions of Mg and Fe in the Octahedral Sheets of Precursor Montmorillonite

The dissolution of 2:1 type phyllosilicates happens mainly at the edges rather than at the basal surfaces under acidic conditions (Rufe & Hochella, 1999; Bickmore et al., 2001). Moreover, a previous study revealed that the transformation mechanism of montmorillonite into kaolinite is probably a local dissolution-recrystallization process which begins mainly at the layer edges, with the complete dissolution of montmorillonite layers occurring within the interstratified kaolinite-montmorillonite (Li et al., 2020). Therefore, the relative concentration changes of dissolved Mg and Fe in the supernatant solutions to some extent represented the contents of released Mg and Fe from the completely dissolved montmorillonite layers, and further reflected the distributions of these two ions in the octahedral sheets.

Cations may be distributed either regularly or randomly in the octahedral sheets of montmorillonite (Vantelon

https://doi.org/10.1007/s42860-021-00138-5 Published online by Cambridge University Press

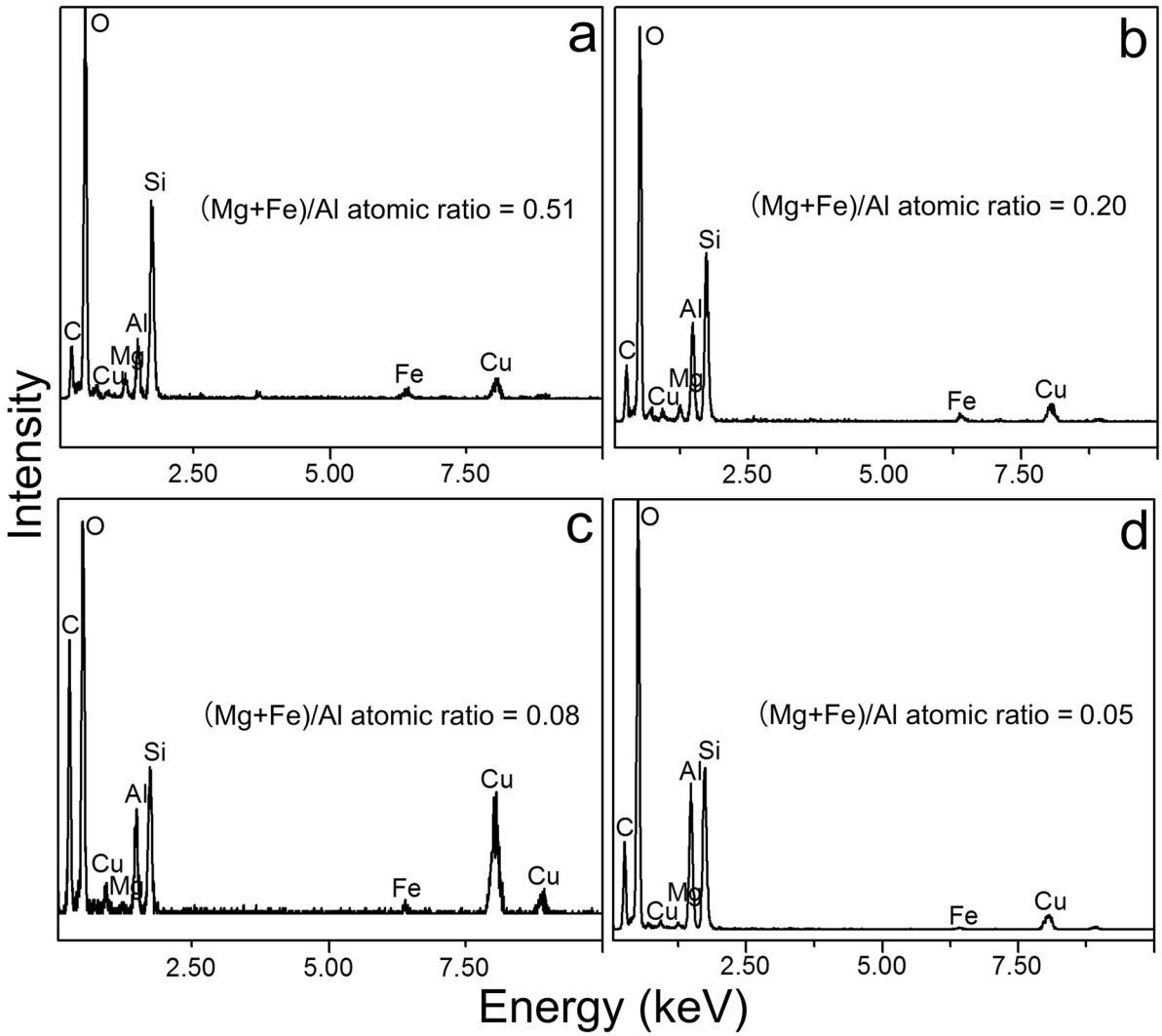

Fig. 6. EDS spectra of montmorillonite and kaolinite particles in the starting material (Mnt) and hydrothermal products. Images **a**, **b**, **c**, and **d** are EDS spectra of the regions surrounded by yellow dotted rectangles in Fig. 5**a**, **b**, **c**, and **d**, respectively

et al., 2001). Assuming that Mg and Fe are distributed regularly in the original montmorillonite, the relative concentrations of Mg and Fe ions should be fixed during the timescale of the hydrothermal experiments. However, compared with the initial stage of transformation, the relative concentrations of Mg and Fe ions reversed in the final stage. This suggested a random distribution of Mg and/or Fe in the octahedral sheets of the montmorillonite, which was consistent with previous studies (Tsipursky & Drits, 1984; Muller et al., 1997; Vantelon et al., 2001).

CONCLUSIONS

A batch of hydrothermal experiments of the transformation of montmorillonite into kaolinite under acidic conditions was carried out to investigate the release relationship between Mg and Fe during such processes. The results showed that iron was ferric and occupied mainly the sites in the octahedral sheets of precursor montmorillonite, which was gradually and nearly simultaneously released along with Mg in the octahedral sheets into solution during the transformation. The concentrations of Mg and Fe ions in the supernatant solutions after hydrothermal reactions indicated that the release rates of Mg and Fe were fast in the initial and final stages but very slow in the intermediate stage. The change in relative concentrations of Mg and Fe ions from initial to final stages suggested that Mg and/or Fe were distributed randomly in the octahedral sheets of the montmorillonite. The insights obtained from this study are helpful in understanding better the release relationship between Mg and Fe during clay-mineral evolution, the distributions of these two elements in the octahedral sheets, and the chemical compositions of clay minerals as indicators of the geological environments.

https://doi.org/10.1007/s42860-021-00138-5 Published online by Cambridge University Press

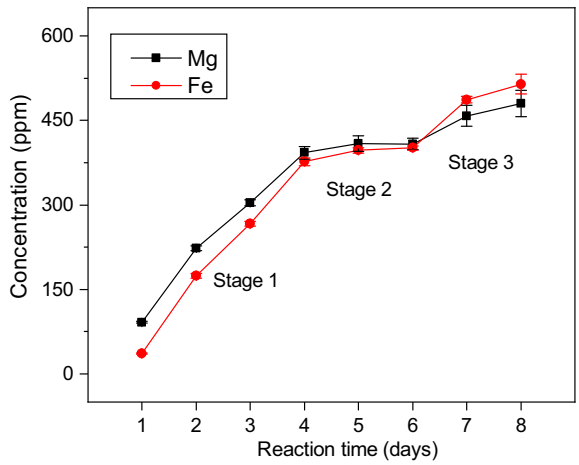

Fig. 7. Concentrations of Mg and Fe in the supernatant solutions of hydrothermal products after various reaction times

ACKNOWLEDGMENTS

The authors sincerely thank the editor-in-chief, associate editor, and the three anonymous reviewers for their valuable comments and suggestions. This work was supported financially by National Key R&D Program of China (Grant No. 2017YFC0602306), National Natural Science Foundation of China (Grant Nos. 41921003, 41825003, and 41772039), Youth Innovation Promotion Association CAS (Grant No. 2018387), the Department of Science and Technology of Guangdong Province (Grant No. 2017GC010128), and Science and Technology Planning Project of Guangdong Province, China (2020B1212060055).

FUNDING

Funding sources are as stated in the Acknowledgments.

Declarations

Conflict of Interest

The authors declare that they have no conflict of interest.

REFERENCES

Adazabra, A. N., Viruthagiri, G., & Shanmugam, N. (2017). Infrared analysis of clay bricks incorporated with spent shea waste from the shea butter industry. *Journal of Environmental Management, 191*, 66–74.

Aparicio, P., & Galan, E. (1999). Mineralogical interference on kaolinite crystallinity index measurements. *Clays and Clay Minerals, 47*, 12–27.

Baron, F., Petit, S., Tertre, E., & Decarreau, A. (2016). Influence of aqueous si and fe speciation on tetrahedral Fe(III) substitutions in nontronites: A clay synthesis approach. *Clays and Clay Minerals, 64*, 230–244.

Baron, F., Petit, S., Pentrak, M., Decarreau, A., & Stucki, J. W. (2017). Revisiting the nontronite Mossbauer spectra. *American Mineralogist, 102*, 1501–1515.

Bickmore, B. R., Bosbach, D., Hochella, M. F., Charlet, L., & Rufe, E. (2001). In situ atomic force microscopy study of hectorite and nontronite dissolution: Implications for phyllosilicate edge surface structures and dissolution mechanisms. *American Mineralogist, 86*, 411–423.

Bray, A. W., Oelkers, E. H., Bonneville, S., Wolff-Boenisch, D., Potts, N. J., Fones, G., & Benning, L. G. (2015). The effect of pH, grain size, and organic ligands on biotite weathering rates. *Geochimica et Cosmochimica Acta, 164*, 127–145.

Cuadros, J., & Dudek, T. (2006). FTIR investigation of the evolution of the octahedral sheet of kaolinite-smectite with progressive kaolinization. *Clays and Clay Minerals., 54*, 1–11.

Cuadros, J., Nieto, F., & Wing-Dudek, T. (2009). Crystal-chemical changes of mixed-layer kaolinite-smectite with progressive kaolinization, as investigated by TEM-AEM and HRTEM. *Clays and Clay Minerals, 57*, 742–750.

Cuevas, J., Leguey, S., Garralon, A., Rastrero, M. R., Procopio, J. R., Sevilla, M. T., Jimenez, N. S., Abad, R. R., & Garrido, A. (2009). Behavior of kaolinite and illite-based clays as landfill barriers. *Applied Clay Science, 42*, 497–509.

Decarreau, A., & Bonnin, D. (1986). Synthesis and crystallogenesis at low-temperature of Fe(III)-smectites by evolution of coprecipitated gels: experiments in partially reducing conditions. *Clay Minerals, 21*, 861–877.

Dong, H. L., Peacor, D. R., & Murphy, S. F. (1998). TEM study of progressive alteration of igneous biotite to kaolinite throughout a weathered soil profile. *Geochimica et Cosmochimica Acta, 62*, 1881–1887.

Doublier, M. P., Roache, T., & Potel, S. (2010). Short-wavelength infrared spectroscopy: A new petrological tool in low-grade to very low-grade pelites. *Geology, 38*, 1031–1034.

Dudek, T., Cuadros, J., & Fiore, S. (2006). Interstratified kaolinite-smectite: Nature of the layers and mechanism of smectite kaolinization. *American Mineralogist, 91*, 159–170.

Dudek, T., Cuadros, J., & Huertas, J. (2007). Structure of mixed-layer kaolinite-smectite and smectite-to-kaolinite transformation mechanism from synthesis experiments. *American Mineralogist, 92*, 179–192.

He, H. P., Guo, J. G., Zhu, J. X., & Hu, C. (2003). ^{29}Si and A^{27} MAS NMR study of the thermal transformations of kaolinite from North China. *Clay Minerals, 38*, 551–559.

He, H. P., Li, T., Tao, Q., Chen, T. H., Zhang, D., Zhu, J. X., Yuan, P., & Zhu, R. L. (2014). Aluminum ion occupancy in the structure of synthetic saponites: Effect on crystallinity. *American Mineralogist, 99*, 109–116.

He, H. P., Ji, S. C., Tao, Q., Zhu, J. X., Chen, T. H., Liang, X. L., Li, Z. H., & Dong, H. L. (2017). Transformation of halloysite and kaolinite into beidellite under hydrothermal condition. *American Mineralogist, 102*, 997–1005.

Hong, H. L., Churchman, G. J., Gu, Y. S., Yin, K., & Wang, C. W. (2012). Kaolinite-smectite mixed-layer clays in the Jiujiang red soils and their climate significance. *Geoderma, 173*, 75–83.

Hong, H. L., Cheng, F., Yin, K., Churchman, G. J., & Wang, C. W. (2015). Three-component mixed-layer illite/smectite/kaolinite (I/S/K) minerals in hydromorphic soils, south China. *American Mineralogist, 100*, 1883–1891.

Hu, X., Lu, G., & Yang, Y. (2000). Determination of cation exchange capacity in clay $[Co(NH3)6]^{3+}$ exchange method. *Chinese Journal of Analytical Chemistry, 28*, 1402–1405 (in Chinese with English abstract).

Ilgen, A. G., Kukkadapu, R. K., Dunphy, D. R., Artyushkova, K., Cerrato, J. M., Kruichak, J. N., Janish, M. T., Sun, C. J., Argo, J. M., & Washington, R. E. (2017). Synthesis and characterization of redox-active ferric nontronite. *Chemical Geology, 470*, 1–12.

Ji, S. C., Zhu, J. X., He, H. P., Tao, Q., Zhu, R. L., Ma, L. Y., Chen, M., Li, S. Y., & Zhou, J. M. (2018). Transformation of serpentine to smectite under hydrothermal condition: Implication for solid-state transformation. *American Mineralogist, 103*, 241–251.

Li, S. Y., He, H. P., Tao, Q., Zhu, J. X., Tan, W., Ji, S. C., Yang, Y. P., & Zhang, C. Q. (2020). Kaolinization of 2:1 type clay minerals with different swelling properties. *American Mineralogist, 105*, 687–696.

Muller, F., Besson, G., Manceau, A., & Drits, V. A. (1997). Distribution of isomorphous cations within octahedral sheets in

https://doi.org/10.1007/s42860-021-00138-5 Published online by Cambridge University Press

montmorillonite from Camp-Bertaux. *Physics & Chemistry of Minerals, 24*, 159–166.

Oliveira, D. P., Sartor, L. R., Souza, V. S., Correa, M. M., Romero, R. E., Andrade, G. R. P., & Ferreira, T. O. (2018). Weathering and clay formation in semi-arid calcareous soils from Northeastern Brazil. *Catena, 162*, 325–332.

Pansu, M., & Gautheyrou, J. (2006). *Handbook of Soil Analysis: Mineralogical, Organic and Inorganic Methods*. Springer.

Rozalén, M. L., Huertas, F. J., Brady, P. V., Cama, J., García-Palma, S., & Linares, J. (2008). Experimental study of the effect of pH on the kinetics of montmorillonite dissolution at 25°C. *Geochimica et Cosmochimica Acta, 72*, 4224–4253.

Rozalén, M. L., Huertas, F. J., & Brady, P. V. (2009). Experimental study of the effect of pH and temperature on the kinetics of montmorillonite dissolution. *Geochimica et Cosmochimica Acta, 73*, 3752–3766.

Rufe, E., & Hochella, M. F. (1999). Quantitative assessment of reactive surface area of phlogopite during acid dissolution. *Science, 285*, 874–876.

Ryan, P. C., & Huertas, F. J. (2009). The temporal evolution of pedogenic Fe-smectite to Fe-kaolin via interstratified kaolin-smectite in a moist tropical soil chronosequence. *Geoderma, 151*, 1–15.

Ryan, P. C., & Huertas, F. J. (2013). Reaction pathways of clay minerals in tropical soils: insights from kaolinite-smectite synthesis experiments. *Clays and Clay Minerals, 61*, 303–318.

Sainz-Diaz, C. I., Timon, V., Botella, V., & Hernandez-Laguna, A. (2000). Isomorphous substitution effect on the vibration frequencies of hydroxyl groups in molecular cluster models of the clay octahedral sheet. *American Mineralogist, 85*, 1038–1045.

Schelz, J. P. (1976). Detection of quartz in clay-minerals by differential thermal-analysis. *Thermochimica Acta, 15*, 17–28.

Tsipursky, S. I., & Drits, V. A. (1984). The distribution of octahedral cations in the 2:1 layers of dioctahedral smectites studied by oblique-texture electron-diffraction. *Clay Minerals, 19*, 177–193.

Vantelon, D., Pelletier, M., Michot, L. J., Barres, O., & Thomas, F. (2001). Fe, Mg and Al distribution in the octahedral sheet of montmorillonites. An infrared study in the OH-bending region. *Clay Minerals, 36*, 369–379.

Zhang, Y., Fu, L. J., & Yang, H. M. (2012). Insights into the physicochemical aspects from natural halloysite to silica nanotubes. *Colloids and Surfaces A: Physicochemical and Engineering Aspects, 414*, 115–119.

Zhang, C. Q., He, H. P., Tao, Q., Ji, S. C., Li, S. Y., Ma, L. Y., Su, X. L., & Zhu, J. X. (2017). Metal occupancy and its influence on thermal stability of synthetic saponites. *Applied Clay Science, 135*, 282–288.

(Received 4 April 2021; revised 26 May 2021; AE: Warren D. Huff)